Amphawan and Fazea *Journal of the European Optical Society-Rapid Publications* (2016) 12:12
DOI 10.1186/s41476-016-0007-7

Journal of the European Optical Society-Rapid Publications

RESEARCH Open Access

Laguerre-Gaussian mode division multiplexing in multimode fiber using SLMs in VCSEL arrays

Angela Amphawan[1,2*] and Yousef Fazea[1]

Abstract

Mode division multiplexing (MDM) is a promising technology for increasing the aggregate bandwidth of multimode fiber (MMF) in conjunction with wavelength division multiplexing (WDM) in face of the impending capacity crunch in optical fiber networks. This paper investigates the effect of radial and azimuthal mode spacings in a 25-channel MDM-WDM system in MMF using a spatial light modulator-controlled VCSEL array for excitation of Laguerre-Gaussian (LG) modes. A data rate of 25Gbps is achieved at a central wavelength of 1550.12 nm. The effects of different azimuthal and radial mode spacings of LG modes are analyzed in terms of the channel impulse response, eye diagram and bit-error rate.

Keywords: Mode division multiplexing, Laguerre-Gaussian mode, Spatial multiplexing, Multimode fiber, Optical fiber communications, Wavelength division multiplexing, Spatial diversity, Parallel computing, Interconnects, Data center

Background

The escalation of network traffic from the profusion of data centers and other cloud computing architectures have catalyzed numerous multiplexing technologies for enhancing the capacity of optical fiber networks and optimizing the optical spectrum. A recent technology for enabling Tb/s optical communications is mode division multiplexing (MDM), which leverages fiber modes as information carriers [1]. The potential of MDM lies in its prowess to break the nonlinear Shannon limit of conventional single-moded optical fiber transmission [2]. In MDM, specific mode or mode groups are used to transmit independent data signals in an optical fiber [3]. By controlling the excitation of modes, the impulse response of each channel may be optimized.

Related work

A prevalent approach for selectively exciting specific modes for different channels is to match the incident field to the inherent modal field of the optical fiber channel using spatial light modulators (SLMs) with different encoding schemes [4–7]. However, alignment may be an issue for developing compact, low-loss systems with separate SLMs.

For better integration and alignment with optical fiber links, all-fiber mode converters have been realized using long-period fiber gratings by CO_2 laser inscription [8, 9], electromagnetic induction [10], mechanical pressure by a metallic grating [11] and by thermal induction [12]. Fiber Bragg gratings have also been used as mode converters by wavelength control of the desired mode based on the reflection spectra [13] and as mode demultiplexers by adjusting the tilt angle to change the coupling efficiencies into different modes at resonant wavelengths on the transmission spectra [14]. VCSEL arrays have been used for generating various incident wavefronts such as Hermite-Gaussian modes [15, 16], donut modes [17, 18], Laguerre-Gaussian modes [16, 19]. For launching orbital angular momentum (OAM) modes, micro-scale spiral-phased plates have been inserted directly into the aperture of a vertical-cavity surface-emitting laser (VCSEL) to promote simple alignment to an optical fiber link when launching orbital angular momentum (OAM) modes [20]. Advancing this further, fiber laser cavities have also been modified to include a photonic crystal grating [21], a long period grating [8] or a fiber Bragg grating [13, 22] to convert the fundamental mode

* Correspondence: angela.amphawan.dr@ieee.org
[1]Optical Computing and Technology Research Laboratory, School of Computing, Universiti Utara Malaysia, Sintok, Kedah, Malaysia
[2]Research Laboratory of Electronics, Massachusetts Institute of Technology, Cambridge, MA, USA

to higher-order modes to allow simultaneous excitation of two or more different modes. Grating-based few mode fiber lasers effectively reduce insertion loss but require high fabrication accuracy and prohibit any change of launch characteristics arising from environmental factors such as bends and strain [23].

Recently, metameterials consisting two concentric rings in a gold film were used to generate OAM modes, where each ring is composed of subwavelength rectangular apertures which function as a localized spatial polarizer [24]. Spiral-phased plates have also been fabricated to generate a coherent superposition of optical vortices with different winding numbers and surface reflection coefficients [25, 26]. In addition, *q*-plates have been fabricated from liquid-crystal slabs to convert a left circularly polarized beam into a helically phased beam with right circular polarization, or vice versa [27]. Furthermore, on-plane mode couplers for combining and separating different spatial channels [28–31], switches for routing different channels [32] have also been developed.

SLMs are versatile and capable of dynamically altering the intensity or/and phase of a beam without moving parts. Adaptive compensation of the wavefront has been demonstrated for real-time micro-alignment of optics in MDM systems, wavefront tuning and interferometry for wavefront verification in MDM systems in order to improve the output power coupling into the desired mode [6, 33, 34]. In [35], an SLM is used to calculate phase masks for each mode using a simulated annealing approach which aims to find the most efficient hologram capable of generating a mode with the highest power coupling efficiency based on the MMF profile. SLMs have also been used for equalization of temporal variations in a MDM system due to the effects of modal dispersion [36–38]. For better digital control of mode purity and alignment, SLMs have recently been incorporated into laser cavities directly. In [39], an integrated system containing a diode-pumped solid state (DPSS) laser where the transverse modes are controlled by an intra-cavity spatial light modulator (SLM) is demonstrated.

Contribution

As an extension to SLM-based MDM techniques above, this paper presents for the first time a numerical model of MDM of Laguerre-Gaussian (LG) modes in multimode fiber (MMF) using integrated SLM-controlled VCSEL arrays. In previous MDM systems, linearly polarized Laguerre-Gaussian modes have been generated using fiber Bragg gratings lasers [40–42], long-period grating lasers [43], separate SLMs [44–47, 7] and photonic crystal fiber [48].

Previous work have addressed the excitation of individual modes and mode groups and its effect on the spatial fields and output power but very little work has addressed the density and spacing between modes. In [49], the mode spacing was designed such that one mode from each of the five nondegenereate mode groups was excited from a customized few mode fiber so as to minimize crosstalk [49]. In [50], mode spacing of a few mode fiber was achieved by rotationally symmetric refractive index perturbations inside the core for varying the sub-group and rotationally nonsymmetric refractive index perturbations in the cladding for varying individual modes. On the other hand, [51] proved experimentally and numerically that the use of a basis set containing optical vortices does not increase the number of degrees of freedom in an optical system.

To the best of the authors' knowledge, this paper presents the first numerical simulation of the effect of mode spacing in SLM-controlled VCSEL arrays for excitation of Laguerre-Gaussian modes in a MMF. The LG mode generation from the SLM is adapted from [52], with the number of lenses reduced to one and the Fourier transform of the desired mode directly displayed on the SLM, encoded in binary phase, so as to obtain the complex field of the desired mode on the Fourier plane by isolating the first diffraction order. The channel degradation is due to mode coupling within the MMF channel. The study evaluates the effect of mode spacing of lower-ordered Laguerre-Gaussian modes on the channel performance by analyzing the effect of different azimuthal mode separations and radial mode number separations on the power coupling coefficients, eye diagrams and bit-error rates from data transmission.

The remainder of the paper is organized as follows. Section 4 describes the mathematical framework and simulation of the MDM design. Section 5 reports on the simulation results and discussion of the results.

Methods

Mode division multiplexing model

The Laguerre-Gaussian MDM model, illustrated in Fig. 1, is simulated using Synopsis Optsim [53] and Mathworks Matlab [54]. Five VCSEL arrays at wavelengths, λ_1 to λ_5 between 1546.92 nm and 1553.33 nm separated by 1.6 nm are used. The optical beam from each VCSEL is expanded and transmitted through a 128x128 pixel transmissive binary amplitude SLM and a lens is placed at its focal length, $f = 300$ mm away from the SLM. Each SLM, k generates 5 modes. The five SLMs are connected to a computer to program the appropriate holograms for generating 25 modes. The LG mode generation from the SLM is adapted from [52], the difference being that the number of lens is reduced to one, thus the Fourier transform of the modal field is displayed directly on the SLM, encoded in binary phase, so as to obtain the complex field of the desired mode as the first diffraction order on the Fourier plane. Let the x-

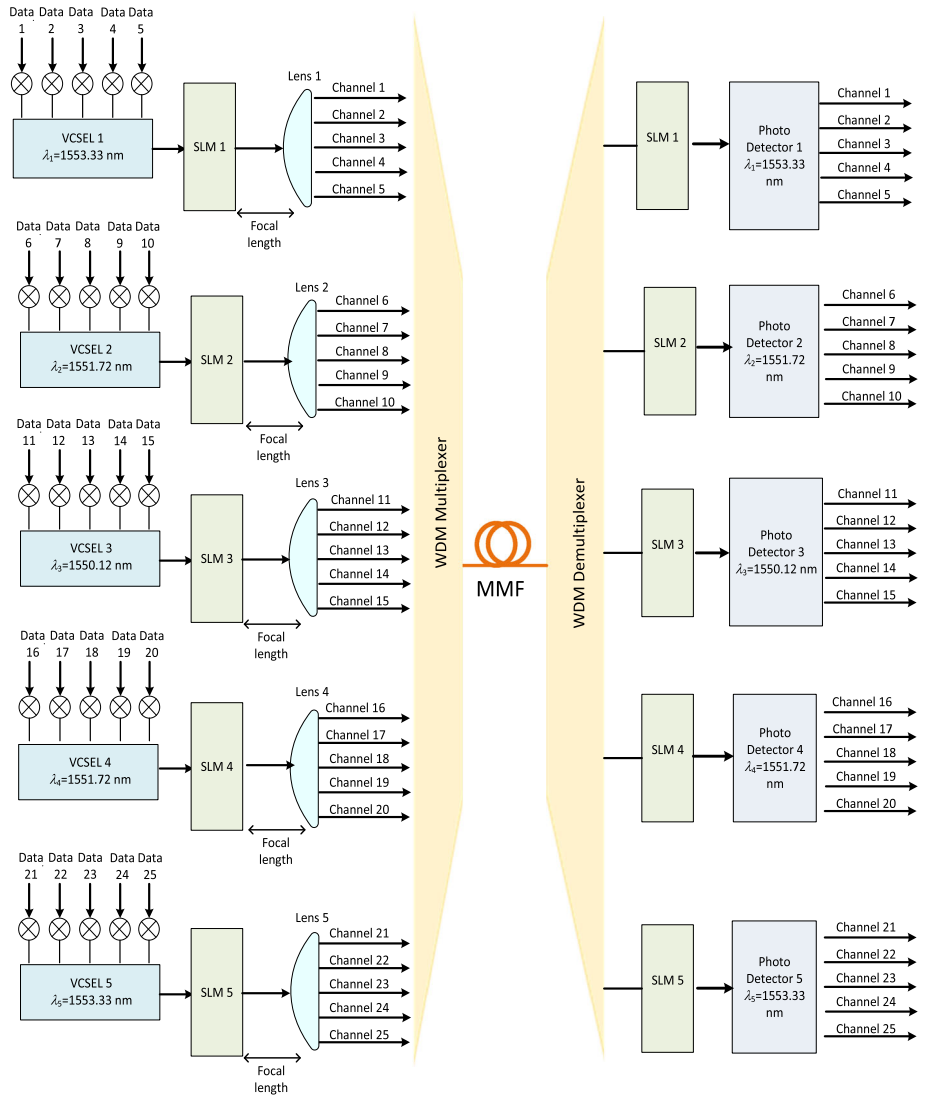

Fig. 1 Laguerre-Gaussian mode division multiplexing model for evaluating the effect of separation of mode numbers on transmission performance

polarized transverse modal field of the c-th LG mode to be derived from the k-th SLM, $E^k_{SLM}(r,\phi)$ be expressed as [55]:

$$E^c_k(r,\phi) = \frac{\exp(-il_c\phi)}{w(\zeta)}\left(\frac{\rho}{w(\zeta)}\right)^{l_c} L^{l_c}_{m_c}\left(\frac{2\rho^2}{w^2(\zeta)}\right)\exp\left(-\frac{\rho^2}{w_o{}^2(1+i\zeta)}\right)\hat{x} \quad (1)$$

where $c = 1, 2, 3, 4, 5$ is the mode index, L^l_m is the generalized Laguerre polynomial [56, 57], $m_c \geq 1$ is the radial mode number for the c-th mode from the k-th SLM, l_c is the azimuthal mode number of the c-th mode from the k-th SLM and $\zeta = z/z_r$ is the reduced coordinates.

Let the Fourier transform of the x-polarization of the transverse modal electric field of each c-th mode from each k-th SLM in Eq. (1) be:

$$d^c_k(x_1,y_1) = F\left[E^c_k(r,\phi)\right] \quad (2)$$

A linear tilt is then added to the Fourier transformed field. This yields the complex field:

$$f^c_k(x_1,y_1) = d^c_k(x_1,y_1)exp\left[j\left(\tau^k_{xc}x + \tau^k_{yc}y\right)\right] \quad (3)$$

where x_1 and y_1 are spatial coordinates, $d^c_k(x_1,y_1)$ is the Fourier transform of the polarized modal electric field of the c-th mode from the k-th SLM; τ^k_{xc} and τ^k_{yc} are linear tilt constants in the horizontal and vertical directions respectively for the c-th mode from the k-th SLM. The

phase of the complex field $f_k^c(x_1, y_1)$ is binarized according to the third type of CGH in [52] and displayed on the SLM, expressed as a Fourier series:

$$g_k^c(x_1, y_1) = a_k^c o + \frac{4}{\pi} \sum_{n=1}^{\infty} a_k^c n \cos\left\{ n \left[\xi(x_1, y_1) + \tau_{xc}^k x + \tau_{xy}^k y_1 \right] \right\} \tag{4}$$

where $a_k^c o$ is the constant term for the c-th mode from the k-th SLM and $a_k^c n = \sin\left[n \alpha_k^c(x_1, y_1)\right]/n$ is the Fourier cosine coefficient of the Fourier series expansion for the c-th mode from the k-th SLM. Each lens then takes the Fourier transform of the binarized modal field on the respective SLM. Taking the Fourier transform of Eq. (4) yields:

$$G_k^c(x_2, y_2) = M_k^c o(x_2, y_2) + \sum_{n=1}^{\infty} [M_k^c n\left(x_2 + n\tau_{xc}^k,\ y_2 + n\tau_y\right) + M_k^c n^*\left(n\tau_x - x_2, n\tau_{yc}^k - y_2\right)] \tag{5}$$

where x_2 and y_2 are spatial coordinates in the Fourier plane of the lens, * is the complex conjugate and $M_k^c n(x_2, y_2)$ is the n-th diffraction order of the c-th mode from the k-th SLM, given by:

$$M_k^c n(x_2, y_2) = F\left\{ a_k^c n(x, y) \right\} = F\left\{ \sin\left[n \alpha_k^c(x_1, y_1)\right] \right\}/n \tag{6}$$

The effect of the tilt is to separate the diffraction orders by multiples of the tilt constants in the Fourier plane and to separate the diffraction orders of the five modes from each SLM. The first diffraction orders of the all c modes from each k-th SLM, $M_k^c 1(x_2, y_2)$ are then spatially isolated by precise coupling into the MMF. The power from each SLM is assumed to be emitted uniformly into five Laguerre-Gaussian modes of spot size 5 μm.

The 25 signals are driven by separate pseudorandom bit sequence (PRBS) offset from one another. After the lenses, the 25 signals are combined using a WDM multiplexer and propagated through a 1 km-long MMF. The refractive index of the MMF is described by [58]:

$$n(R) = n_{co}(1 - \Delta R^{\alpha}) \tag{7}$$

where n_{co} is the maximum refractive index of the core, R is the normalized radial distance from the center of the core, Δ is the profile height parameter and α is the profile alpha parameter of the refractive index. The total incident spatial electric field at the MMF input is expressed as:

$$E_{lm}^i(r,\ \phi,\ t) = E_{lm}^i(t) E_{lm}^i(r,\ \phi) = \left[\sum_l \sum_m c_{lm} e_{lm}(t) \right] E_{lm}^i(r, \phi). \tag{8}$$

The total output field is the sum of fields generated by each fiber mode in addition to phase delay proportional to the propagation constant, given by:

$$E_{out}(r,\ \phi,\ t) = \sum_l \sum_m c_{lm} e_{lm}\left(t - \tau_q\right) E_{lm}^i(r, \phi) \exp\left(j\beta_q z\right) \tag{9}$$

where τ_q and β_q are the time delay and propagation constant respectively of the degenerate mode group, q. Each fiber mode will experience mode attenuation, accounted by [59]:

$$\gamma = \gamma_0 \left\{ 1 + I_p \left[\eta \left(\lambda(|l| + 2m)/(2\pi R n_{co})[(\alpha + 2)/(\alpha\Delta)]^{1/2} \right)^{\frac{2\alpha}{\alpha+2}} \right] \right\} \tag{10}$$

where γ_0 is the basic attenuation seen by all modes, I_p is the p-th order modified Bessel function of the first kind, η is a scaling factor. Chromatic dispersion is described by:

$$D(\lambda) = (S_0 \lambda/4)\left(1 - {\lambda_0}^4/\lambda^4\right) \tag{11}$$

where λ is the operating wavelength of interest, λ_0 is the zero dispersion wavelength and S_o is the dispersion slope at λ_0.

Power modal coupling, caused by micro-bending and perturbations of the optical fiber cross-section, is assumed to lead to nearest-neighbor coupling and solved iteratively using [60]:

$$\frac{\partial P_q}{\partial z} + \tau_q \frac{\partial P_q}{\partial t} = -\alpha_q P_q + \kappa_q d_q \left(P_{q+1} - P_q\right) - \gamma_{q-1} d_{q-1} \left(P_q - P_{q-1}\right) \tag{12}$$

where $P_q(z,\ t)$ is the average power signal for mode group q, v_q is the mode group velocity, α_q is the power attenuation coefficient for mode group q, k_q and γ_q are degeneracy factors for the number of modes exchanging power between mode groups q and q +1; d_q is the mode-coupling coefficient between mode groups q and $q + 1$ governed by:

$$d_q = \frac{1}{8} \left(\frac{2\pi n_{co} \rho}{\lambda} \right) \left(\frac{q}{q_{\max}} \right)^{\frac{4}{\alpha+2}} \frac{C_o}{\Delta {\beta_q}^{2p}} \tag{13}$$

where C_o is a mode-coupling factor, p is the phenomenological parameter, $\Delta\beta_q$ is the difference in average propagation constants between mode groups $q + 1$ and q. At the receiver, nointerferometric modal decomposition [61] is performed to demultiplex the modes before photodetection for each of the five wavelengths.

Investigation of mode spacing

To evaluate the effect of mode spacing on the system performance, four cases were analyzed:

1. Fixed radial mode number $m = 1$ and azimuthal mode number spacing, $\Delta l = 1, 2, 3, 4, 5$
2. Fixed radial mode number $m = 3$ and azimuthal mode number spacing, $\Delta l = 1, 2, 3, 4, 5$
3. Fixed azimuthal mode number $l = 1$ and radial mode number spacing, $\Delta m = 1, 2, 3, 4, 5$
4. Fixed azimuthal mode number $l = 3$ and radial mode number spacing, $\Delta m = 1, 2, 3, 4, 5$

As an example, the modes contained for each azimuthal mode number spacing for the first case is shown in Table 1.

The signal from each VCSEL is then demultiplexed into five separate channels. The channel impulse response is computed from the power coupling coefficient, c_{lm} [56]:

$$c_{lm} = \int_0^{2\pi} \int_0^{\infty} E_{lm}^{o}(r, \phi) \cdot e_{lm}^{*}(r, \phi) \cdot r \; dr \, d\phi \qquad (14)$$

where $E_{lm}^{o}(r, \phi)$ is the output electric field and e_{lm} is the transverse electric field of LG modes. For the worst-case scenario, complete redistribution of power is assumed to take place immediately after the generated modal field is coupled into the MMF.

The channel impulse response, eye diagrams, and BER for each channel is examined for different MMF lengths and discussed in the next section

Results and Discussions

Figures 2 and 3 shows the average BER per photodetector array with respect to MMF length for azimuthal mode number separations $\Delta l = 1, 2, 3, 4, 5$ for fixed radial mode numbers, $m = 1$ and $m = 3$ respectively. It is observed that as a whole, the average BER per photodetector array when $m = 1$ is better than the average BER per VCSEL for $m = 3$. Due to larger distances between the lobes in the transverse electric field profile for $m = 3$ compared to $m = 1$ and higher similarity of spatial fields for higher-order modes, for $m = 3$, the possibility of mode coupling into adjacent modes is higher

Table 1 Azimuthal mode numbers contained for various azimuthal mode number spacings Δl

Azimuthal Mode Number Spacing, Δl	Azimuthal Mode Numbers, l
1	l = 1, 2, 3, 4, 5
2	l = 1, 3, 5, 7, 9
3	l = 1, 4, 7, 10, 13
4	l = 1, 5, 9, 13, 17
5	l = 1, 6, 11, 16, 21

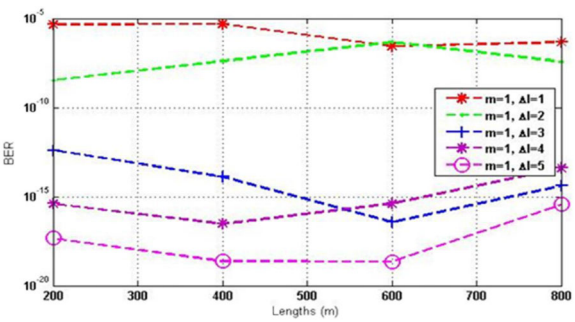

Fig. 2 Effect of spacing of azimuthal mode order, Δ*l* and MMF length on BER when $m = 1$

than the possibility of mode coupling into adjacent modes for $m = 1$. For $m = 1$, when $\Delta l = 2$ and $\Delta l = 3$, the BER reduces for a MMF length of 0 m to 600 m but for $\Delta l = 1$, 4 and 5, the BER increases for a MMF length of 0 m to 600 m. Mode coupling starts to occur between 500 m to 600 m, causing the BER to gradually equalize for all Δl values due to reduced differential mode delays. Beyond 600 m, for $m = 1$, mode coupling increases with distance. On the other hand, for $m = 3$, the BER is overall poor except for $\Delta l = 5$ when the BER is acceptable. This demonstrates that the separation of azimuthal mode numbers is insignificant when the radial mode number is increased.

Figure 4 shows the channel impulse response when the radial mode number is fixed at 1 and the azimuthal mode number spacing is varied. In Fig. 4(a) and (b), the power is coupled into both higher-order modes and lower-order modes. Hence, the time delay between highly coupled modes is large, resulting in large differential mode delays and high BERs of 6.15×10^{-7} when $\Delta l = 1$ for Fig. 4(a) and 7.87×10^{-8} for $\Delta l = 2$ in Fig. 4(b). In Fig. 4(c), (d) and (e), the power is mostly coupled into higher order modes producing narrow pulses and low BERs. When $\Delta l = 3$ in Fig. 4(c), a BER of 3.87×10^{-14} is achieved, whereas for $\Delta l = 4$ in Fig. 4(d) and $\Delta l = 5$ in Fig. 4(e), BER values of 6.53×10^{-13} and 5.05×10^{-16} are achieved respectively. Moreover, the curve of the channel impulse response is left-skewed with

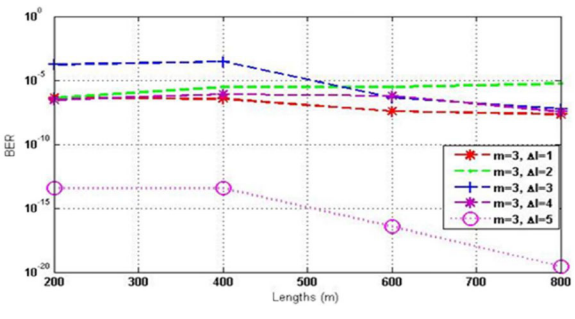

Fig. 3 Effect of spacing of azimuthal mode order, Δ*l* and MMF length on BER when $m = 3$

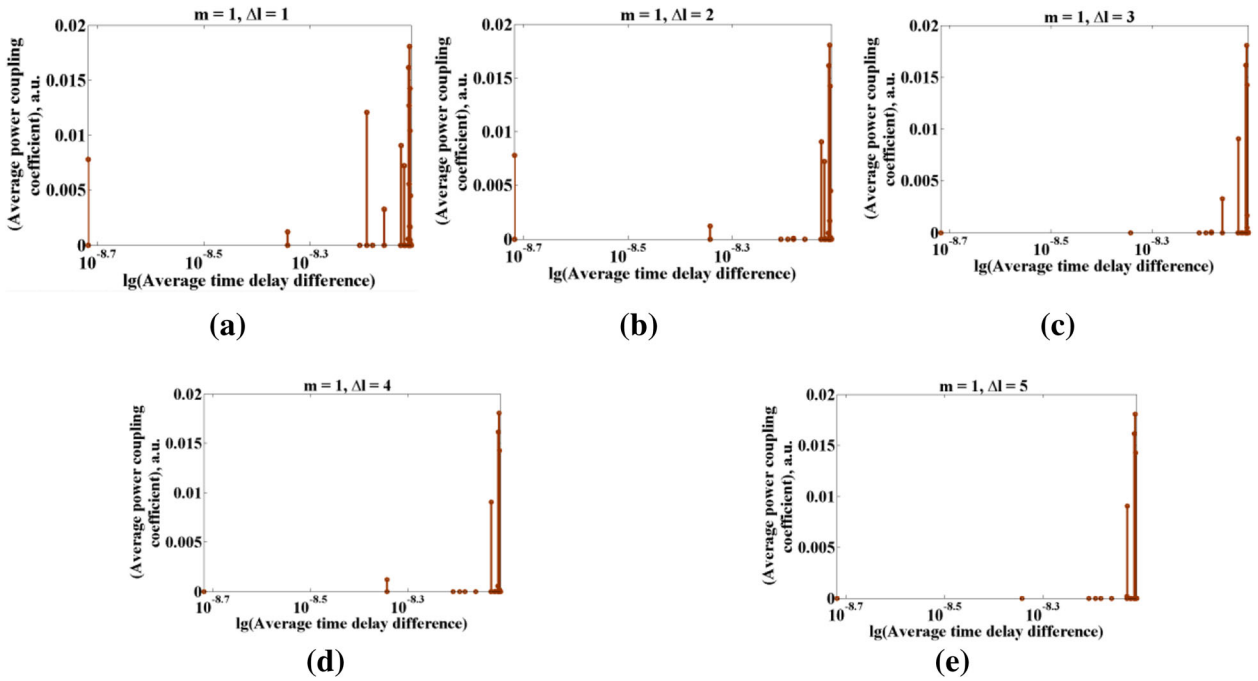

Fig. 4 Effect of mode delay of azimuthal mode number when radial mode number $m = 1$ and the azimuthal mode number separation Δl is varied: (**a**) $\Delta l = 1$, (**b**) $\Delta l = 2$, (**c**) $\Delta l = 3$, (**d**) $\Delta l = 4$ and (**e**) $\Delta l = 5$

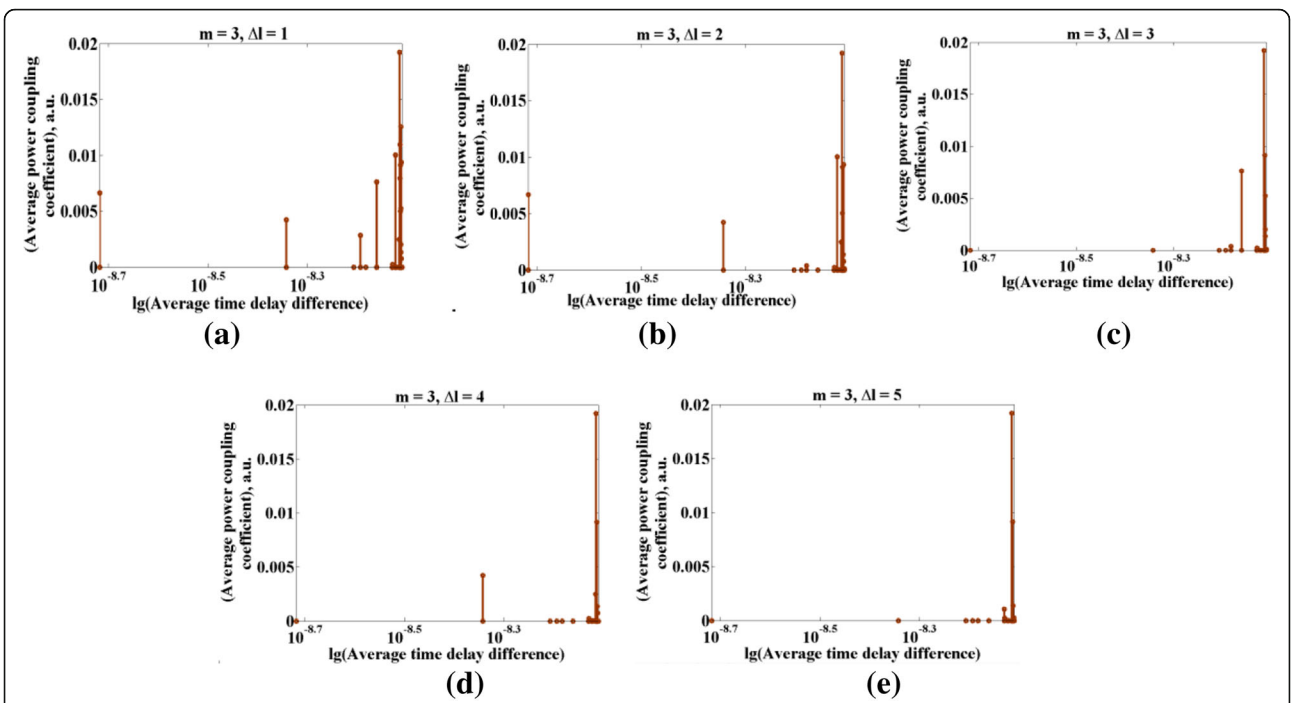

Fig. 5 Effect of mode delay of azimuthal mode number when radial mode number $m = 1$ and the azimuthal mode number separation Δl is varied: (**a**) $\Delta l = 1$, (**b**) $\Delta l = 2$, (**c**) $\Delta l = 3$, (**d**) $\Delta l = 4$ and (**e**) $\Delta l = 5$

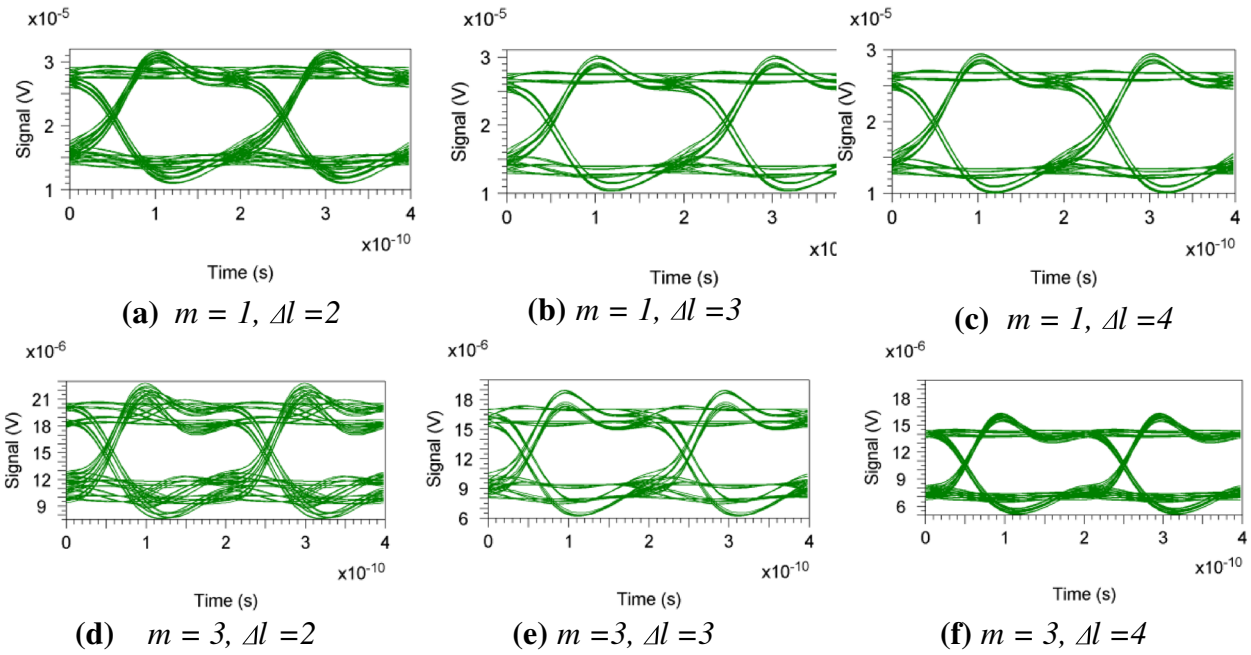

Fig. 6 Eye diagram at $\lambda = 1550.12\ nm$ for various azimuthal mode spacings when radial mode number is fixed: (**a**) m = 1, Δl = 2 (**b**) m = 1, Δl = 3 (**c**) m = 1, Δl = 4 (**d**) m = 3, Δl = 2 (**e**) m = 3, Δl = 3 (**f**) m = 3, Δl = 4

power dominating higher-order modes for cases Fig. 4(c), (d), and (e). This is in contrast to the channel impulse response in MDM in [62] where the power is distributed more symmetrically across all modes.

Figure 5 shows the channel impulse response when the radial mode number is fixed at 3 and the azimuthal mode number is varied. Figure 5(a) and (b) show that most power is highly coupled in higher-order modes. Some suppression of medium-order modes and strong suppression of lower-order modes is observed. Hence, the time delay between modes is rather large, resulting in a large pulse width. This is confirmed by the BER measurements whereby for case $\Delta l = 1$ in Fig. 5(a), BER = 4.98×10^{-7} and for $\Delta l = 2$ in Fig. 5(b), BER = 8.02×10^{-8}. In Fig. 5(c) for $\Delta l = 3$, the power is mostly coupled into higher-order modes with stronger suppression of medium-order modes and lower-order modes compared to Fig. 5(a) and (b), producing a narrow pulse width and a lower BER value of 4.86×10^{-9}. In Fig. 5(d) for $\Delta l = 4$, the modes are more scrambled and the power is distributed to higher modes and medium-order modes resulting in a larger pulse width and a lower BER value of 2.60×10^{-8} compared to the BER for $\Delta l = 3$. In Fig. 5(e) for $\Delta l = 5$, the power is dominantly coupled in higher-order modes only, producing the smallest pulse width and achieving the lowest BER value of 3.54×10^{-17}. The power is coupled predominantly in higher-order modes for cases (c), and (e). This is in contrast to the channel impulse response of MDM in [62] where the power is spread more uniformly across all modes.

Figure 6 shows a comparison of the eye diagrams showing the effect of azimuthal mode number separation Δl for fixed values of m at a MMF length of 400 m. In the first row of Fig. 6 when the radial mode number is maintained to $m = 1$, as Δl increases, the time deviation between propagation modes is reduced and the eye opening increases. In the second row for $m = 3$, a similar pattern is observed as Δl increases. The largest eye opening is achieved when $\Delta l = 5$.

Comparison of the average BER versus length for various mode number spacings, Δm is reported in Figs. 7 and 8 for fixed azimuthal mode number of $l = 1$ and $l = 2$ respectively. For both l =1 and $l = 3$, BER values for even values of Δm are better than the BER values for odd values of Δm. For even values of Δm, the polarities of

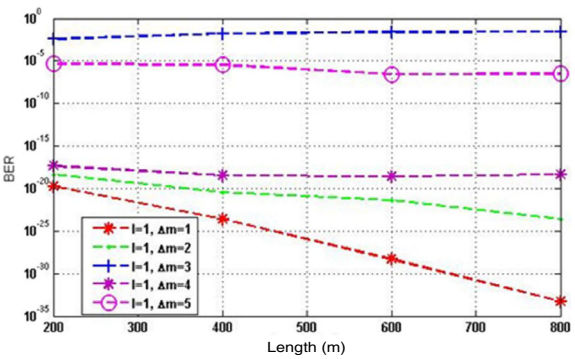

Fig. 7 Effect of spacing of radial mode order spacing Δm and MMF length on BER when $l = 1$

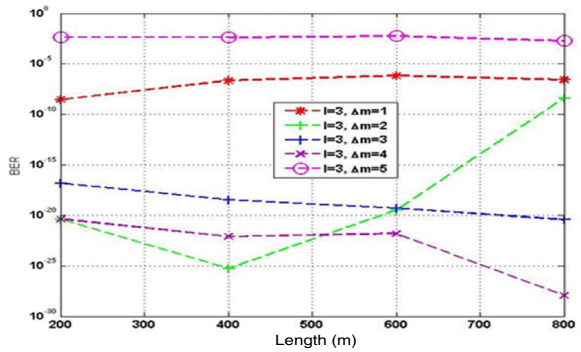

Fig. 8 Effect of spacing of radial mode order spacing Δm and MMF length on BER when $l = 3$

the peaks of spatial fields cancel each other due to the complementary phases. For odd values of Δm, the polarities of the peaks of the spatial fields are out of phase with one another. Due to the effect of the polarity differences, the BER for the cases of $\Delta m = 3$ and $\Delta m = 5$ are lower than the BER of even values of. Δm. Also, interestingly, the BER for $l = 1$ generally decreases for all Δm values whereas for $l = 3$, the BER decreases for all Δm values except for $\Delta m = 2$. This is potentially due to the similarity between the inherent transverse electric field of modes of radial mode numbers spacings of 2 and 4.

The channel impulse responses for the investigation of the effect of radial mode order spacing Δm is shown in Figs. 9 and 10 for fixed azimuthal mode orders $l = 1$ and $l = 3$ respectively. In Fig. 9(a) and (b), the power is coupled predominantly into higher range modes. Hence, the time delay is very low resulting in a narrow pulse. For $\Delta m = 1$ in Fig. 9(a), a BER of 6.88×10^{-31} is exhibited whereas for $\Delta m = 2$ in Fig. 9(b), a BER of 3.03×10^{-20} is attained. In Fig. 9(c) for $\Delta m = 3$, the power is spread across medium-ordered modes, leading to a large delay spread between modes, thus attaining a low BER of 1.69×10^{-2}. In Fig. 9(d) for $\Delta m = 4$ and Fig. 9(e) for $\Delta m = 5$, the power is dominantly coupled in higher-order modes. Hence, the delay spread between modes is very low, attaining a BER o f 2.87×10^{-17} and BER of 4.61×10^{-9} for $\Delta m = 4$ and $\Delta m = 5$ respectively. The power dominates in higher-order modes for cases (a), (b), (d) and (f). Thus, in our MDM model, due to the suppression of lower-order modes, the time delay between modes is minimized compared to [62].

The effect of radial mode order spacing Δm when the azimuthal radial number $l = 3$ is shown in Fig. 10. Strong coupling into higher-order modes and high suppression of medium-ordered modes and lower-order modes are exhibited in Fig. 10(a), (b), (c) and (d). Hence, the time delay variation between modes is low, resulting in a narrow pulse. Figure 10(a) $\Delta m = 1$ exhibits a BER of 1.81×10^{-9}, Fig. 10(b) $\Delta m = 2$ exhibits a BER of 9.31×10^{-10}, Fig. 10(c) $\Delta m = 3$ exhibits a BER of 2.91×10^{-21} and Fig. 10(d) $\Delta m = 4$ exhibits a BER of 5.08×10^{-29}. In Fig. 10(e) for $\Delta m = 5$, the power is coupled into medium-order modes and simultaneously distributed in the lower and higher-order modes. Hence, the time delay between

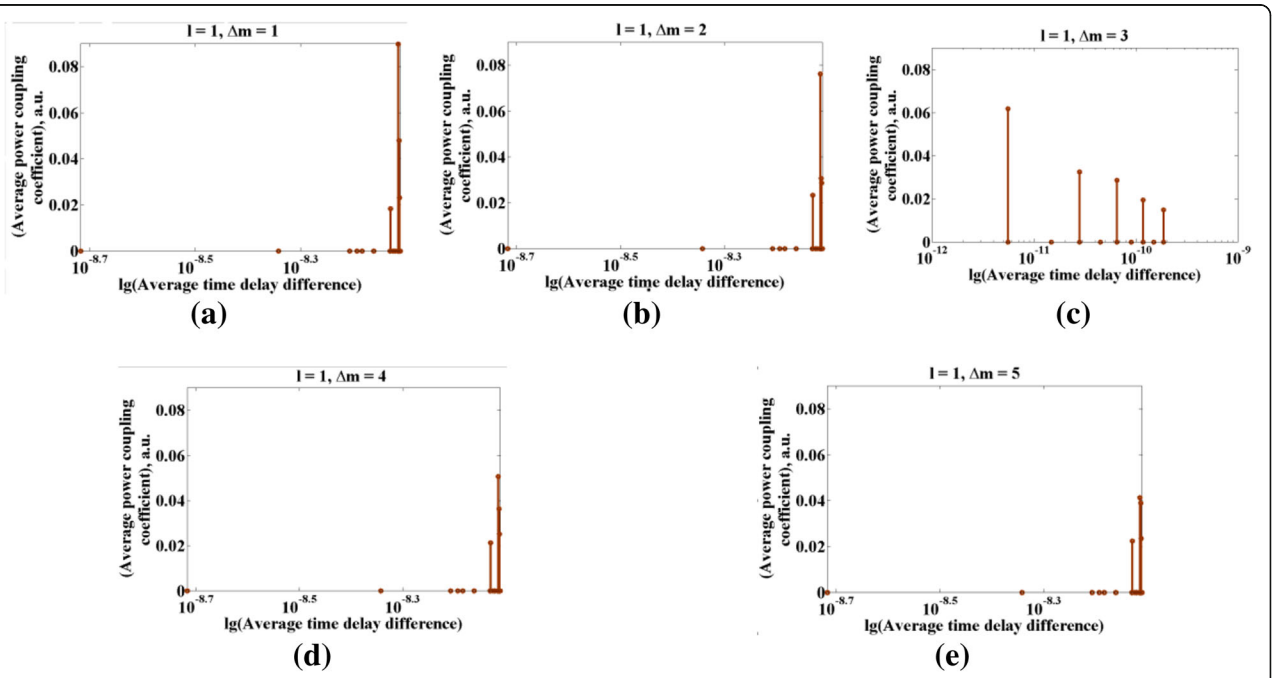

Fig. 9 Channel impulse response for $l = 1$ when radial mode number spacing Δm is varied: (**a**) $\Delta m = 1$, (**b**) $\Delta m = 2$, (**c**) $\Delta m = 3$, (**d**) $\Delta m = 4$ (**e**) $\Delta m = 5$

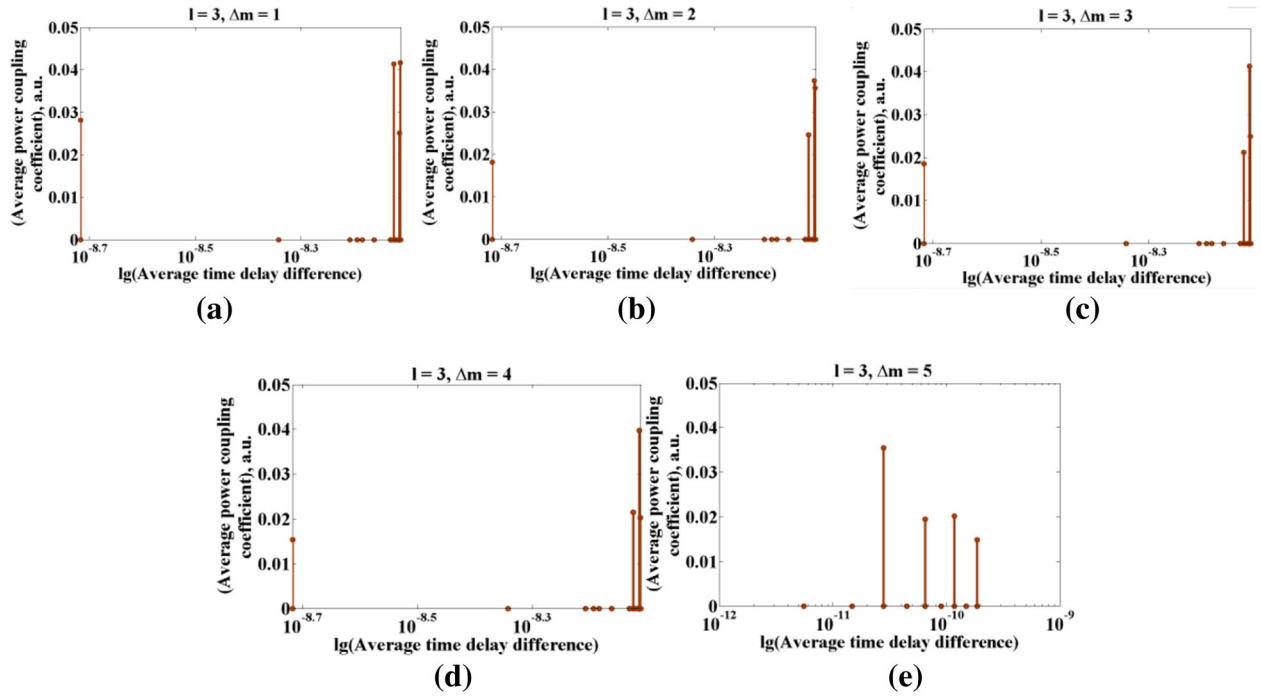

Fig. 10 Channel impulse response for $l = 3$ when radial mode number spacing Δm is varied: (**a**) Δm = 1, (**b**) Δm = 2, (**c**) Δm =3, (**d**) Δm = 4 (**e**) Δm = *5*

modes is large resulting in a wide pulse width and a low BER of 4.65×10^{-2}.

Figure 11 shows a comparison of the eye diagrams showing the effect of radial mode number separation for MMF length of 400 m when the azimuthal mode number is fixed. The first row for fixed azimuthal mode number $l = 1$ shows that when Δm is even, the eye opening is fairly wide compared to when Δm odd. The same pattern is observed for fixed azimuthal mode number $l = 3$. The eye opening is better for even Δm's as more of

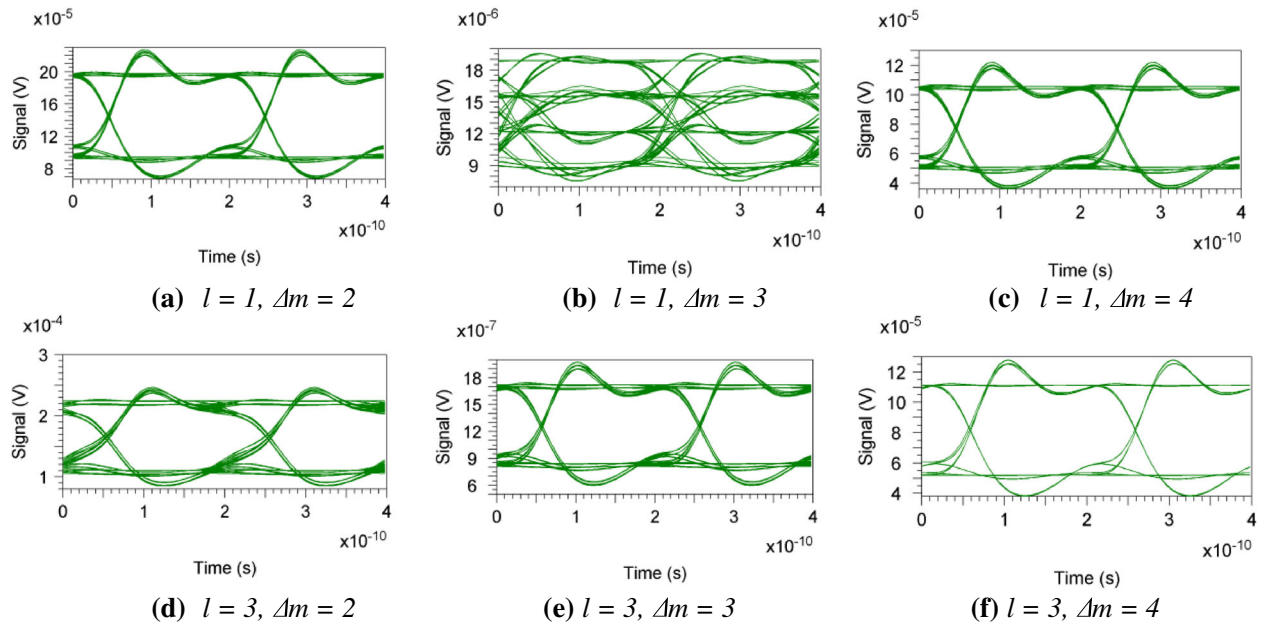

Fig. 11 Eye diagrams at λ = 1550.12 nm showing the effect of radial mode number separation at a length of 400 m when the azimuthal mode number is fixed: (**a**) l = 1, Δm = 2 (**b**) l = 1, Δm = 3 (**c**) l = 1, Δm = 4 (**d**) l = 3, Δm = 2 (**e**) l = 3, Δm = 3 (**f**) l = 3, Δm = 4

the output modes are from the same degenerate mode group.

The results may be generalized to other experimental setups for exciting LG modes using different SLM encoding schemes, gratings, VCSEL arrays and masks in a MMF. However, the results may not be generalized for other types of modes such as HG and OAM modes in MMF. Also, the results may not be generalized to the propagation of LG modes in free-space as atmospheric conditions may affect the mode number separations differently from the mode coupling mechanism in MMF.

Conclusions

In this paper, a 25Gbps 25-channel MDM-WDM model has been numerically simulated at a center wavelength of 1550.12 nm multiplexing five Laguerre-Gaussian modes on each of the five SLM-controlled VCSEL arrays separated in wavelength by 1.6 nm. Rigorous performance analyses of the effect of mode spacings show that it is possible to attain a narrow channel impulse response and an acceptable BER by maintaining a low radial mode number up to 3 and ensuring that the mode spacing of the azimuthal mode number is higher than 4; or by maintaining a low azimuthal mode number up to 3 and using an even radial mode number separation. The work may provide valuable insight into possible configuration of mode numbers for increasing channel diversity in dense optical interconnects for data centers.

Acknowledgements

The authors would like to express their sincere gratitude to Prof. Vincent Chan and Prof. Jeffrey Shapiro at the Research Laboratory of Electronics, Massachusetts Institute of Technology for their valuable technical discussions and constructive feedback on the research. The first author gratefully acknowledges the United States Department of States for the Fulbright Award.

Author's contributions

The original idea, mathematical framework, experiment and simulation model were developed by the first author. The second author worked on the simulations and evaluation. The progress is a result of common contributions and discussions. Both authors read and approved the final manuscript.

Competing interests

The authors declare that they have no competing interests.

Received: 2 February 2016 Accepted: 12 May 2016
Published online: 05 September 2016

References

1. Pile D. Integrated photonics: Compact multiplexing. Nat Photon. 2015;9:78.
2. Winzer PJ. Spatial multiplexing: The next frontier in network capacity scaling. In: Optical Communication (ECOC 2013), 39th European Conference and Exhibition on. 2013. p. 1–4.
3. Amphawan A. Review of optical multiple-input–multiple-output techniques in multimode fiber. Opt Eng. 2011;50:102001.
4. Bozinovic N, Yue Y, Ren Y, Tur M, Kristensen P, Huang H, et al. Terabit-Scale Orbital Angular Momentum Mode Division Multiplexing in Fibers. Science. 2013;340:1545–8.
5. Carpenter J, Wilkinson TD. All Optical Mode-Multiplexing Using Holography and Multimode Fiber Couplers. J Light Technol. 2012;30:1978–84.
6. Amphawan A. Holographic mode-selective launch for bandwidth enhancement in multimode fiber. Opt Exp. 2011;19:9056–65.
7. Amphawan A. Binary spatial amplitude modulation of continuous transverse modal electric field using a single lens for mode selectivity in multimode fiber. J Mod Opt. 2012;59:460–9.
8. Jiangli D, Kin Seng C. Temperature-Insensitive Mode Converters With CO_2 –Laser Written Long-Period Fiber Gratings. IEEE Photon Technol Lett. 2015; 27:1006–9.
9. Xiaoyong Z, Yiping W, Changrui L, Guolu Y, Jiangtao Z, Guanjun W, et al. Long Period Fiber Gratings Inscribed With an Improved Two-Dimensional Scanning Technique. IEEE Photon J. 2014;6:1–8.
10. Sakata H, Sano H, Harada T. Tunable mode converter using electromagnet-induced long-period grating in two-mode fiber. Opt Fiber Technol. 2014;20:224–7.
11. An L, Xi C, Al Amin A, Jia Y, Shieh W. Space-Division Multiplexed High-Speed Superchannel Transmission Over Few-Mode Fiber. J Light Technol. 2012;30:3953–64.
12. Gruner-Nielsen L, Nicholson JW. Stable mode converter for conversion between LP < inf > 01</inf > and LP < inf > 11</inf > using a thermally induced long period grating. In: Photonics Society Summer Topical Meeting Series, 2012 IEEE. 2012. p. 214–5.
13. Jiangli D, Kin Seng C. Mode-Locked Fiber Laser With Transverse-Mode Selection Based on a Two-Mode FBG. IEEE Photon Technol Lett. 2014;26:1766–9.
14. Gao Y, Sun J, Chen G, Sima C. Demonstration of simultaneous mode conversion and demultiplexing for mode and wavelength division multiplexing systems based on tilted few-mode fiber Bragg gratings. Opt Express. 2015;23:9959–67.
15. Amphawan A, Fazea Y and Ibrahim H: Investigation of Channel Spacing for Hermite-Gaussian Mode Division Multiplexing in Multimode Fiber. In: IEEE International Colloquium on Signal Processing and its Applications (CSPA), Kuala Lumpur (2015)
16. Amphawan A, Fazea Y, Elshaikh M, Sulaiman AH, Othman AM, Othman IMF, Rahim AY, Pee CN. Space Division Multiplexing in Multimode Fiber for Channel Diversity in Data Communications. In: Advanced Computer and Communication Engineering Technology: Proceedings of ICOCOE 2015. Cham: Springer International Publishing; 2016. p. 355–63.
17. Amphawan A, Fazea Y, Elfouly T, Abualsaud K. Effect of Vortex Order on Helical-Phased Donut Mode Launch in Multimode Fiber. Adv Sci Lett. 2015; 21:3042–5.
18. Amphawan A, Fazea Y and Ibrahim H: Mode division multiplexing of spiral-phased donut modes in multimode fiber. In: International Conference on Optical and Photonic Engineering (icOPEN 2015), pp. 95240S-95240S-6. Singapore (2015)
19. Fazea Y and Amphawan A: Mode Division Multiplexing of Helical-Phased LG Modes in MMF with Electronic Dispersion Compensation. Adv. Sci. Lett. 2016. in press
20. Li H, Phillips DB, Wang X, Ho Y-LD, Chen L, Zhou X, et al. Orbital angular momentum vertical-cavity surface-emitting lasers. Optica. 2015;2:547–52.
21. Lin D, Xia K, Li J, Li R, Ueda K-i, Li G, et al. Efficient, high-power, and radially polarized fiber laser. Opt Lett. 2010;35:2290–2.
22. Dong J, Chiang KS. Transverse-mode switchable passively mode-locked fiber laser based on a two-mode fiber Bragg grating. In: 19th Optoelectronics and Communications Conference (OECC) and the 39th Australian Conference on Optical Fibre Technology (ACOFT). 2015. p. 65–7.
23. Ndagano B, Brüning R, McLaren M, Duparré M, Forbes A. Fiber propagation of vector modes. Opt Express. 2015;23:17330–6.
24. Zhao Z, Wang J, Li S, Willner AE. Metamaterials-based broadband generation of orbital angular momentum carrying vector beams. Opt Lett. 2013;38:932–4.
25. Rumala YS, Leanhardt AE. Multiple-beam interference in a spiral phase plate. J Opt Soc Am B. 2013;30:615–21.
26. Rumala YS. Propagation of structured light beams after multiple reflections in a spiral phase plate. Opt Eng. 2015;54:111306.
27. Lorenzo M, Ebrahim K, Sergei S, Bruno P, Enrico S, Eleonora N, et al. Spin-to-orbital conversion of the angular momentum of light and its classical and quantum applications. J Opt. 2011;13:064001.
28. Riesen N, Love JD. Design of mode-sorting asymmetric Y-junctions. Appl Opt. 2012;51:2778–83.
29. Ding Y, Xu J, Da Ros F, Huang B, Ou H, Peucheret C. On-chip two-mode division multiplexing using tapered directional coupler-based mode multiplexer and demultiplexer. Opt Express. 2013;21:10376–82.

30. Veldhuis GJ, Berends JH, Lambeck PV. Design and characterization of a mode-splitting Ψ-junction. J Light Technol. 1996;14:1746–52.
31. Amphawan A, Samman NMAA and Nedniyom B: Selective excitation of LP01 mode in multimode fiber using solid-core photonic crystal fiber. J. Mod. Opt. 2013;60
32. Stern B, Zhu X, Chen CP, Tzuang LD, Cardenas J, Bergman K, et al. On-chip mode-division multiplexing switch. Optica. 2015;2:530–5.
33. Amphawan A, Mishra V, Nisar K, Nedniyom B. Real-time holographic backlighting positioning sensor for enhanced power coupling efficiency into selective launches in multimode fiber. J Mod Opt. 2012;50:1745–52.
34. Amphawan A. Binary encoded computer generated holograms for temporal phase shifting. Opt Exp. 2011;19:23085–96.
35. Carpenter, J and Wilkinson, TD: Precise modal excitation in multimode fibre for control of modal dispersion and mode-group division multiplexing. In: European Conf. and Exposition on Optical Communications (ECOC), p. We. 10.P1. Geneva (2011)
36. Arik SO, Kahn JM, Ho K-P. MIMO Signal Processing for Mode-Division Multiplexing: An overview of channel models and signal processing architectures. IEEE Signal Proc Mag. 2014;31:25–34.
37. Neng B, Guifang L. Adaptive Frequency-Domain Equalization for Mode-Division Multiplexed Transmission. IEEE Photon Technol Lett. 2012;24:1918–21.
38. Arık SÖ, Askarov D, Kahn JM. Adaptive Frequency-Domain Equalization in Mode-Division Multiplexing Systems. J Light Technol. 2014;32:1841–52.
39. Brüning R, Ngcobo S, Duparré M, Forbes A. Direct fiber excitation with a digitally controlled solid state laser source. Opt Lett. 2015;40:435–8.
40. Sun B, Wang A, Xu L, Gu C, Zhou Y, Lin Z, et al. Transverse mode switchable fiber laser through wavelength tuning. Opt Lett. 2013;38:667–9.
41. Dong J, Chiang KS. Mode-locked fiber laser with transverse-mode selection based on a two-mode FBG. IEEE Photon Technol Lett. 2014;26:1766–9.
42. Sun B, Wang A, Gu C, Chen G, Xu L, Chung D, et al. Mode-locked all-fiber laser producing radially polarized rectangular pulses. Opt Lett. 2015;40: 1691–4.
43. Dong J, Chiang KS. Temperature-Insensitive Mode Converters With CO 2-Laser Written Long-Period Fiber Gratings. IEEE Photon Technol Lett. 2015;27: 1006–9.
44. Jung, Y-M, Li, Z, Wong, NHL, Daniel, J, Sahu, JK, Alam, S, et al: Spatial mode switchable, wavelength tunable erbium doped fiber laser incorporating a spatial light modulator. In: Optical Fiber Communication Conference, p. Tu3D.4. San Francisco, California; (2014)
45. Amphawan A. Holographic mode-selective launch for bandwidth enhancement in multimode fiber. Opt Express. 2011;19:9056–65.
46. Amphawan A. Backlighting for alignment of optics in first diffraction order path. In: Int. Conf. on Applications of Optics and Photon. 2011. p. 8001–237.
47. Amphawan A and Brien DO. Holographic mode field generation for a multimode fiber channel, "International Conference on Photonics, 2010, pp. 1–4.
48. Amphawan A, Nedniyom B, Al Samman NMA. Selective excitation of LP01 mode in multimode fiber using solid-core photonic crystal fiber. J Mod Opt. 2013;60:1675–83.
49. Robert B, Bienvenu N, Melanie M, Siegmund S, Jens K, Michael D, et al. Data transmission with twisted light through a free-space to fiber optical communication link. J Opt. 2016;18:03LT01.
50. May AR, Zervas MN. Few-mode fibers with improved mode spacing. In: Optical Communication (ECOC), 2015 European Conference on. 2015. p. 1–3.
51. Chen M, Dholakia K, Mazilu M. Is there an optimal basis to maximise optical information transfer? Sci Rep. 2016;6:22821.
52. Arrizón V, Ruiz U, Carrada R, González LA. Pixelated phase computer holograms for the accurate encoding of scalar complex fields. J Opt Soc Am A. 2007;24:3500–7.
53. Synopsis. OptSim. ed, 2010.
54. Mathworks. MATLAB. vol. 2013, 2013 ed. Natick, MA, USA, 2013.
55. Pampaloni F, Enderlein J. Unified operator approach for deriving Hermite–Gaussian and Laguerre–Gaussian laser modes. J Opt Soc Am A. 2004;21: 1553–8.
56. Abramowitz M, Stegun IA. Handbook of mathematical functions : with formulas, graphs and mathematical tables. New York: Dover Publications; 1973 [9th Dover printing, with additional corr.].
57. Amphawan A and Alabdalleh WA. Simulation of Properties of the Transverse Modal Electric Field of an Infinite Parabolic Multimode Fiber. Microw Opt Lett. 2012;54:1362–1365.
58. Snyder AW, Love JD. Optical waveguide theory. London: Chapman and Hall; 1983.
59. Olshansky R, Oaks SM. Differential mode attenuation measurements in graded-index fibers. Appl Opt. 1978;17:1830–5.
60. Yadlowsky J, Mickelson AR. Distributed loss and mode coupling and their effect on time-dependent propagation in multimode fibers. Appl Opt. 1993; 32:6664–77.
61. Amphawan A, O'Brien D. Modal decomposition of output field for holographic mode field generation in a multimode fiber channel. In: Photonics (ICP), 2010 International Conference on. 2010. p. 1–5.
62. Shi K, Feng F, Gordon G, Wilkinson T and Thomsen B. SLM-based Mode Division Multiplexing System with 6× 6 Sparse Equalization. IEEE Photon. Tech. Lett., vol.27, pp. 1687-1690 (2015)